Increasing Light Absorption and Collection Using Engineered Structures

Yasir J. Noori, Christopher S. Woodhead and
Robert J. Young

Additional information is available at the end of the chapter

Abstract

In recent years we have witnessed an explosion of interest in two dimensional (2D) materials, due to their unique physical properties. Excitement surrounds the promise of replacing conventional bulk photodetectors with devices based on 2D materials, allowing better integration, flexibility and potentially improving performance. However, the low inherent light absorption of 2D materials is an outstanding issue to be solved. In this chapter we review two independent approaches to tackling this problem, which have the potential to be combined to find a robust solution. The first approach involves patterning the substrate with a rod-type photonic crystal (PhC) cavity structure, which is shown to increase the light absorption into a 2D material flake coupled spatially to the cavity mode. Secondly, we review 2D–compatible solid immersion lenses (SILs) and their ability to increase both the optical magnification of the structures they encapsulate, and the longevity of the material. SILs have been shown to reduce the requirements for complex optics in the implementation of 2D materials in optoelectronic devices, and also in preserving the photodetector's optical performance over long periods of time. Finally, we show how by combining rod-type PhC cavities with SILs, we can improve the performance of 2D material-based photodetectors.

Keywords: rod-type photonic crystals, quality factor, solid immersion lenses, epoxy

1. Introduction

Two-dimensional transition metal dichalcogenides (TMDs) are a class of semiconducting materials, which can be exploited for a range of diverse applications [1]. Their ultra-thin dimensions and novel properties can provide unique advantages in fields such as energy [2, 3], computing [4–6] optoelectronics [7, 8], sensing [9, 10] and security [11, 12]. Current

bottlenecks in commercialising devices formed from TMDs are their relatively poor quantum yield, low optical absorption and high rate of degradation in ambient conditions. The quantum yield of TMDs, namely the number of excitons generated divided by the number of photons impinged on the device, is typically between 0.01 and 6% [13], which is exceptionally low in comparison to other emitters such as III-V based structures that can have quantum yields reaching close to 100% [14, 15].

TMD monolayers such as MoS_2 have excellent absorption characteristics [16], and high photo-responsivity [9] relative to their dimensions. However, their extreme thinness of just 0.65 nm means that the absolute absorption is usually relatively low (typically less than 6% at 450 nm) [17] severely limiting the efficiency of TMDs in real implementations such as detectors and solar cells. This value can be increased by using multiple monolayers, [17] or by careful preparation of the incident light [18]; however such methods may not be practical for specific optoelectronic applications.

Multiple existing approaches have been developed to circumvent these limitations. One method involves the use of superacid treatment to obtain near a 100% photoluminescence quantum yield from these materials [13, 19]. Currently, reports of superacid treatment have all involved using Bis(trifluoromethane) sulfonimide as the superacid material for treating MoS_2. The photoluminescence intensity of MoS_2 monolayers have been shown to increase up to 190-fold after treatment [13]. While the explanation of the enhancement in light emission as a result of superacid treatment is still not very clear, recent studies demonstrated that enhancement could be caused by the transformation of trions into neutral excitons combined with a reduction in the density of mid-gap trap states for CVD grown monolayers [20].

Improved monolayer absorption can be achieved by coupling TMD monolayers to an engineered structure that confines plasmonic modes such as gold nanostructures [21, 22], nanoparticles [23] and nanorods [24, 25]. This phenomenon stems from the fact that plasmonic resonance couples to both excitation and emission fields, hence boosting the light-matter interaction at the nanoscale. For example, Johnson et al. have observed a giant enhancement in the luminescence intensity of tungsten diselenide (WSe_2) by coupling it to plasmonic structures, resulting in an increased light absorption [26]. They report achieving an enhancement factor of up to 200 using silver nanotriangle arrays coupled to the monolayers. Sobhani et al. in [23] have observed that by tuning plasmonic core-shell nanoparticles to the direct bandgap of monolayer MoS_2 and depositing them sparsely onto the monolayer's surface, the photocurrent achieved through the monolayer increases 3-fold, hence promising a model for more sensitive TMD based photodetectors. Other structures such as nanocubes [27] and bowtie antennae [28, 29] have also been utilized for enhancing light emission, resulting in up to 2000 fold increase in material's absorption.

Absorption of TMD monolayers can also be increased when they are coupled to photonic crystal (PhC) structures such as cavities, which can greatly aid in improving the efficiency of photodetectors [30, 31]. Like plasmonic structures, the strong localization of electromagnetic radiation in photonic cavities increases the light-matter interaction, leading to higher absorption efficiency. For example, by monolithically integrating graphene with a Fabry-Perot microcavity, the optical absorption can be enhanced by 26-fold, reaching absorption values

greater than 60% [32]. Combining graphene with hole-type PhC cavities, has been shown to increase light reflectivity from graphene by 4.0x [33]. A photodetector can be realized by fabricating metal contacts above sheets, through which a circuit current can be amplified and measured when the device is illuminated.

An alternative method for enhancing monolayer light absorption using PhCs was proposed by Noori et al. in [31]. In this method, a rod-type PhC is used to achieve an increased light to monolayer coupling. This PhC can be combined with a high refractive index solid immersion lens (SIL) [34, 35], which is placed directly above the cavity. This has two effects: the first is to act as a reflective interface to redirect any leaking light back into the cavity, increasing the chance of light absorption by the monolayer. The second is to increase the coupling of light into/out of the cavity, increasing the probability that an applied photon gets into the cavity, which SILs are considered especially effective at [36, 37]. SILs are commonly made out of glass [36], which can pose a problem when integrating into delicate structures such as PhCs and 2D materials. Recent work forming SILs out of photopolymers, has shown progress in solving this issue [38–40].

For the rest of this chapter, we will focus on the concept of a rod-SIL photodetector. We will review the rod-based PhC structure and compare it to the more common method of coupling monolayers to uncapped hole-type PhCs. We will then look at photopolymer based solid immersion lenses, and their effectiveness at both coupling light into/out of a material, as well as protecting it from the ambient environment. Finally, we discuss how the combination of the two structures can provide an efficient optical package for use in photodetection.

2. Enhancing light absorption using photonic crystal cavities

2.1. Coupling 2D materials to photonic crystals

In 1987, Yablonovitch proposed the theoretical concept of using periodic optical structures to create photonic bandgap systems, now popularly known as photonic crystals [41]. A PhC structure comprises of a series of periodic changes in refractive index that creates a range of disallowed states for a photon, effectively forming a photonic bandgap. This effect is very similar to electronic bandgaps experienced by electrons in an atomic lattice, thus PhCs are sometimes describes as 'optical lattices'.

Experimental realization of manmade PhCs occurred a decade later [42, 43]. Ever since that time, PhCs became a potential platform for making integrated photonic components such as cavities, waveguides, mirrors and wavelength/polarization multiplexers [44, 45]. This allows the realization of technologies such as single photon sources, lasers, filters, interferometers, modulators and slow light waveguides.

Coupling 2D materials to photonic cavities can lead to substantial improvements in the material's absorption efficiency, opening the doors for their use in the development of ultrathin but highly efficient detectors. TMD monolayers have also been coupled to hole-type PhC cavities, resulting in lasing and enhancement in the spontaneous emission rate for light emitted

from these 2D materials [46–50]. Hole-type PhC cavities can have high Q-factors due to their reduced mode losses in the vertical direction due to the refractive index contrast at the bridge-air interface. However, the hole-type PhCs have distinct disadvantages when being used with non-embedded emitters such as 2D materials, because the cavity mode is confined within the bridge structure; a region where the TMD monolayer cannot realistically be placed. This causes reduced coupling between the photo-absorber monolayer and the cavity mode's maximum, leading to a reduction in light-matter interactions. Secondly, the large dielectric-to-air volume ratio that exists in the structures of hole-type PhCs results in undesirable light absorption by the dielectric material. This becomes critical when a high absorption material, such as GaAs, is used with an operating wavelength that lies in the visible regime. However, a lot of these issues can be solved by changing the PhC structure from a hole-type to a rod-type [31].

2.2. Photonic crystal cavity design

PhC structures are commonly formed from a hexagonal array structure, rather than a square array because, they are easier to fabricate in practice [51]. For rod-type cavities, square lattice arrays exhibit a transverse magnetic (TM) bandgap with Q-factors that may exceed 1000. However, confining light in the visible wavelength range using the square lattice PhC requires the structure to have feature sizes that may be difficult to fabricate using conventional lithography techniques. For example, assume a square lattice PhC is designed for the optical bandgap of monolayer molybdenum disulfide (MoS_2), i.e. approximately 660 nm [52]; Villeneuve et al. in [51] showed that for a rod-type PhC lattice with material index $n = 3.4$, $a = 1$ and $r = 0.2a$, a H1 cavity would have its cavity mode at $\lambda = 2.56a$. In other words, a PhC cavity with a mode at $\lambda = 660\,nm$, requires its lattice constant to be, $a = 258\,nm$ and the radius to be, $r = 52\,nm$, with rod heights of at least 660 nm. Designing rods with such dimensions is challenging and requires extreme controllability of the fabrication process. Furthermore, small fabrication uncertainties that change the rods' radius, the lattice constant, sidewall roughness and/or their vertical height can shift the cavity mode and change its Q-factor. An H1 hexagonal lattice PhC cavity of similar dimensions has its cavity mode at a much smaller wavelength. Hence, a cavity designed to have a mode wavelength at 660 nm will have larger dimensions, making it less dependent on fabrication limitations. The cavity that will be discussed in this chapter can achieve this goal using $a = 595\,nm$ and $r = 95\,nm$, which are easier to achieve in practice.

The PhC studied here consists of a hexagonal lattice of rods surrounded by air for, optimum index contrast. Since MoS_2 has an absorption wavelength at 660 nm, due to its direct bandgap, rods made from common substrates such as silicon or GaAs can have a refractive index that exceeds 3.5 at this wavelength. To make the photonic cavity, a rod is omitted from the PhC lattice allowing a photonic state to be created within the lattice's photonic bandgap. The confined wavelength of the cavity is also known as the cavity mode. In previous work by Kay et al. [53], 2D materials have been shown to dip when transferred onto hollowed regions such as etched trenches on a substrate. Through exploiting the flexibility of TMD monolayers, spatial coupling between the cavity and the material is possible by suspending the monolayer over the rods; **Figure 1** illustrates this concept. Having a sufficient lattice separation, the cavity region, can allow the suspended flake to sag within the cavity such that the flake's

topological minimum spatially matches the cavity mode's antinode. Optimized alignment in both position and energy optimizes absorption by the 2D material. The PhC hexagonal lattice is surrounded by air for optimum index contrast. MoS_2 is the material considered here for this work because of its large neutral and charged exciton binding energies, making it a great candidate for room temperature photodetection. Nevertheless, the PhC design is universal, as the normalized parameters may be scaled and adjusted to match any light absorptive TMD. It consists of rods with a lattice constant, $a = 1$, and a radius, $r = 0.165a$, where the rods are made by etching the silicon substrate.

2.3. Cavity performance

2D PWE simulations of the PhC structure (**Figure 2a**), have shown that a bandgap exists in the frequency range $1.05a < \lambda < 1.17a$. Once the photonic band diagram was simulated, a H1 cavity was formed in the centre of the array. Subsequently, FDTD is commonly used to test the cavity's performance. 2D simulations can confirm the presence of the cavity mode and used to analyze its central wavelength. Performing 2D simulations at this point can usually save a lot of computation time and power that may be spent with exhaustive 3D simulations. Q-factor measurements from 2D simulations typically show astronomical values since leakage in the vertical direction is not included.

3D FDTD simulations of the cavity mode are shown in **Figure 2b** and **c**. Initially, an E_x polarised source was placed at the center of the cavity, with a central wavelength λ of $1.1a$ and a full-width at half maximum (FWHM) of $d\lambda = 0.1a$. Using Meep, a visual image of the light propagation can be produced. After allowing enough time to pass following initialization of the dipole, to allow edge states and propagating modes to leak, the cavity standing mode's field was observed on its own, as shown in **Figure 3a**. The cavity is later simulated with an E_y
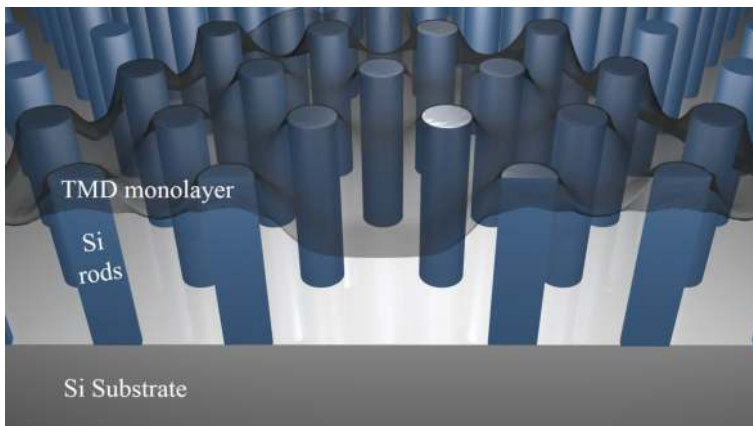

Figure 1. Cross-sectional illustration of a silicon rod PhC cavity with a monolayer transferred on top. Declining of the monolayer within the cavity region can increase coupling between excitons and the cavity modes.
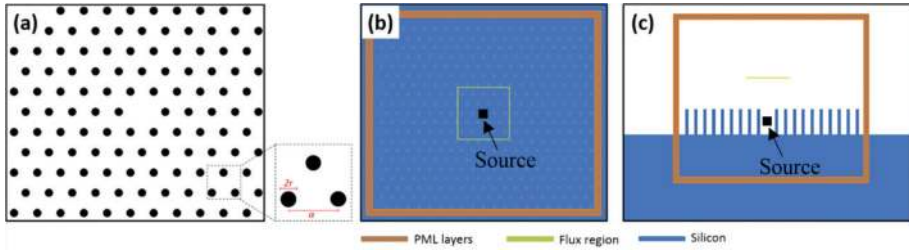
Figure 2. (a) An x-y cross-section of the simulated PhC cavity structure. x-y (b) and y-z (c) screenshots of the simulated structure from Lumerical FDTD package showing the PM layers and flux region.
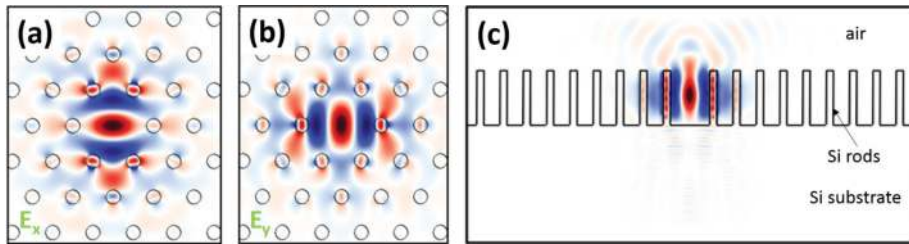

Figure 3. 3D FDTD simulation of the photonic cavity mode showing time slice images of the confined E_x (a) and E_y (b) components. (c) Cross section of the E_y field within the microcavity. Red (blue) represents positive (negative) components of the electric field.

polarised dipole, which showed an electric field distribution for the cavity mode, as shown in **Figure 3b**. Using the harmonic inversion (harminv) tool embedded in Meep, the cavity mode was found to have a wavelength λ = 1.12a with a Q-factor of 300. On the other hand, **Figure 3c** shows the field distribution for a cross-sectional slice along the x-direction through the cavity. Unsurprisingly, the PhC rod's height also influences the mode's confinement. If the rods are too short, the cavity mode's shape can extend into the air above the PhC. This results in a reduction in the spatial interface between the mode and the rods, lowering the light collection ratio. Conversely, if the rods are too long, higher order and propagating modes can form within the cavity structure. Furthermore, etching high aspect ratio rods will always require complex dry etching techniques to achieve the desired degree of anisotropy. It has been revealed that maximum gap size for a square-lattice rod-type PhC is achieved for rod heights of approximately 2.3a, corresponding to approximately two cavity modes wavelengths [51].

The Q-factor of a cavity can be defined as the ratio of the energy stored in the resonating cavity to the energy dissipated per cycle. For a cavity with a Q-factor of 300, such as the rod-type PhC cavity discussed here, a resonating photonic mode inside a cavity is expected to oscillate 300 times before it leaks half of its energy outside the cavity. For a MoS$_2$ monolayer with an absorption coefficient of 0.05, coupled to a rod-type PhC cavity the absorption of the monolayer can be enhanced to almost unity [52]. This can be calculated using the following equation:

$$\alpha_c = 1 - (\alpha_m)^{Q_c} \tag{1}$$

where α_c is the absorption of a monolayer that is coupled to a cavity, α_m is the absorption of a monolayer that is not coupled to a cavity and Q_c is the cavity's Q-factor. Note that in this approximation, absorption due to the dielectric host material (in this case considered silicon) was not taken into account. It is expected that absorption due to the material can reduce the cavity's Q, however this becomes less critical for cavities designed to have low-mid Q-factors such as the ones shown here where light is allowed to leak into the cavity to enhance absorption for optimized photodetection.

A series of simulations were carried out with a source inside a PhC cavity containing rods with different radii. The aim is primarily to investigate the robustness of this design to fabrication imperfections that are likely to occur due to the relatively small structure. Causes of shifts in the radius of the fabricated rods could be due to the inaccurate selection of exposure dosage in the electron-beam (e-beam) writing process. Other reasons could be due to non-anisotropic sidewall profile development of the exposed regions of the resist, due to temperature variations of the developing solution and/or the samples themselves. Hence, the radius was varied between $0.155a$ and $0.170a$. **Figure 2b** and **c** show screenshots taken directly from Lumerical's user interface for the simulation cell. The mesh resolution used in this simulation is 20 elements per one lattice constant, a, in every dimension. Corresponding to approximately one element per 30 nm in real units. To measure the cavity mode, a flux region was setup above the cavity, collecting light from the cavity mode radiated vertically upward. A maximum Q-factor of 341 was achieved for a PhC cavity having rods with a radius, $r = 0.161a$, where the cavity mode's central wavelength is $\lambda = 1.104a$, as shown in **Figure 4**. As the radius deviates from $r = 0.161a$, the collected power flux starts to decrease, which results from a decrease in the Q-factor, recording a minimum of 155 at $\lambda = 1.138a$ for $r = 0.170a$. It is clear from **Figure 4** to note that reducing the radius of the rods tends to blue-shift the cavity mode's energy, hence reducing its wavelength. This is expected, as the relationship between the PhC's cell radius (hole-type or rod-type) and the cavity mode's wavelength was anticipated through previous studies [54]. **Figure 4** plots a comparison between the obtained fluxes for two cases. The first case is when a flake is exfoliated directly onto a flat substrate. The second case is when the flake is transferred on top of the PhC structure, dipping to half the height of the rods where the cavity's field maximum exists for rods with $r = 0.161a$. Later, the effect of having the source away from the cavity's centre will be discussed.

Throughout the scope of this work, the simulations were made with the assumption that the flake is dipped to about half the height of the rods. This is expected to be the ideal case since the flake will be coupled to the field's antinode, creating maximal spatial coupling to the cavity. Performing simulations to anticipate the amount of dipping of a monolayer over a typical structure depends on many factors. These include the monolayer material, the rods' surface roughness, temperature, etc. These typically require setting up finite element simulations while taking into account the van der Waals, Coulombic and gravitational forces, which is very exhaustive. Hence, a series of simulations were run to investigate the effect of dipping of the monolayer emitter on the monolayer-cavity coupling. These simulations are done
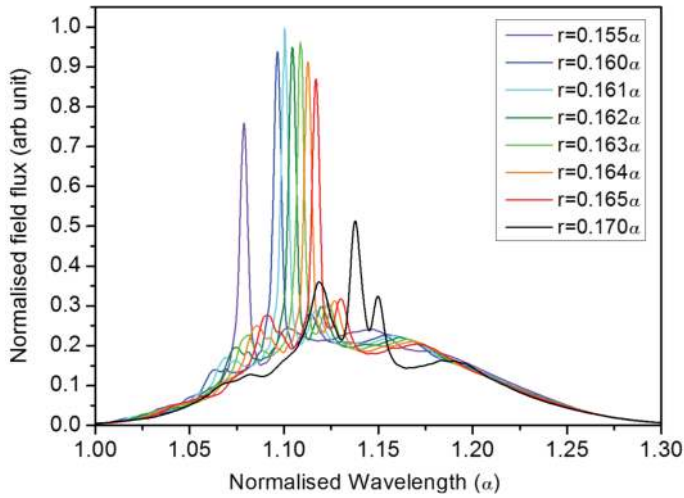
Figure 4. The effect of changing the rods' radii r from 0.155a to 0.170a on the cavity mode, showing a maximum Q for r = 0.161a and an increase in the cavity's central wavelength when r is increased, and vice versa.
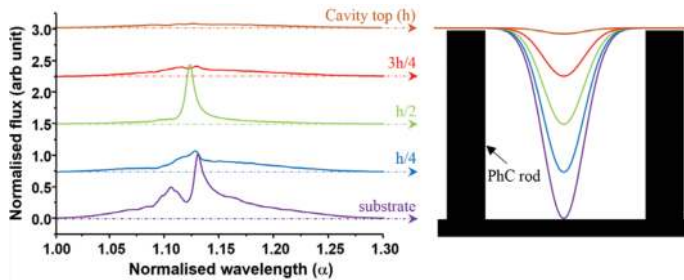

Figure 5. Comparison of the flux spectra for emission from the cavity as the dipping of the material is varied along the z-axis. The drawing on the right illustrates the degrees of bowing of the 2D material from the surface of the structure into the cavity for each of the cases shown on the left.

by placing the dipole at different heights along the vertical direction inside the cavity. Even though the source position in the vertical direction was changed along the height of the cavity, it is important to mention that the flux region height above the photonic structure was not changed. The cavity spectra for the different heights are shown in **Figure 5**. It is expected that maximum absorption of the monolayer should be achieved when the source is spatially aligned with the cavity mode's electric field maximum. This exists at the center of the cavity, one wavelength above the substrate, as was previously shown in **Figure 3c**. The intensity of the cavity mode was found to decrease as the source is moved toward the top of the rods due to reduced spatial coupling between the dipole source and the cavity mode's antinode, which exists in the center of the cavity.

Compared to H1 cavities, L3 cavities are usually favored for better coupling to PhC wave-guides and tend to have lower confinement quality factors of roughly 150. In L3 cavities, the Q-factor is expected to reduce due to increased coupling of the cavity mode to radiative modes.

Having an engineered structure that can improve absorption of monolayers is essential, in the next section we will describe how a different structure such as a micro-lens can help increase the light collection efficiency to these monolayers/cavity systems.

3. Enhancing light collection using photopolymer lenses

A solid immersion lens (SIL) is an optical element with a high refractive index that can be placed on the surface of a semiconductor to increase the optical extraction efficiency of a surface/subsurface emitter. SILs are typically formed from high index glass [55] and are placed directly on the surface of an optical structure to increase the light being coupled into and/or out from it. SILs can also be formed from photopolymers such as UV-curable epoxy [40], which gives the SIL unique properties such as easy tunability and mounting. The rest of this section will focus on these types of SILs.

Two different geometries of SIL have been predominantly studied; those with a hemispherical shape (h-SILs) and those with a Weierstraß shape (s-SILs) [55], as shown **Figure 6**. S-SILs have a higher magnification than h-SILs, scaling as the refractive index of the SIL squared as opposed to a direct linear relationship for a h-SIL. In subsurface emitters such as quantum dots (QD's), s-SILs have a higher input/output coupling efficiency over h-SILs, due to them being able to refract a higher number of rays at the SIL-air boundary, thus collecting/delivering a greater solid angle of light (θ_s) to and from a device. In the case of a surface emitter such as a 2D material this SIL-air boundary refraction in the s-SIL is essential to increase the input/output coupling, as there is no contribution to light coupling from the substrate-SIL boundary.
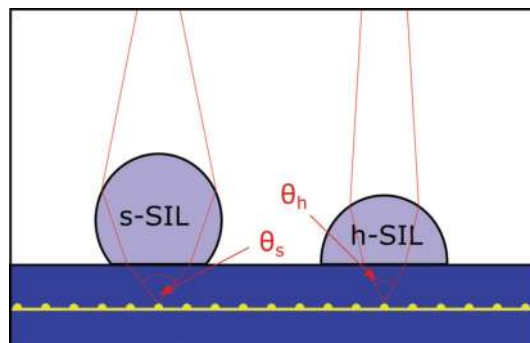

Figure 6. Diagram showing the difference in shape between a s-SIL and h-SIL on a sample with embedded emitters (quantum dots) in the above case (yellow features). The dashed lines highlight how a larger angle of emitted light is collected in the s-SIL relative to the h-SIL.

3.1. SIL fabrication

The process of creating an epoxy SIL onto a 2D material is described in this chapter. The sample containing the 2D material is immersed into a glycerol bath, which provides the liquid phase medium needed to enable the formation of droplets with high contact angles, such as the SILs those shown in **Figure 6**. This arises due to a modification of the surface tension experienced by the droplet, and can be explained by considering the Young equation given in (2) [56] and illustrated in **Figure 7**.

$$\cos\theta_y = \frac{\gamma_{sf} - \gamma_{sl}}{\gamma_{lf}} \tag{2}$$

where γ_{sf}, γ_{sl} and γ_{lf} are the solid-filler, solid–liquid and liquid-filler surface tensions, respectively. When the filler solution is air, γ_{sf} is greater than both γ_{sl}, and γ_{lf}. This makes $cos(\theta y) > 0$, resulting in a small equilibrium contact angle (θy). However, when a filler solution such as glycerol is used, γ_{sf} reduces dramatically, allowing $cos(\theta y) < 0$; this allows droplets with a contact angle over 90 degrees to form. Glycerol is an ideal filler solution due to it being relatively inert with respect to the epoxy. Other filler solutions such as water are less ideal as they are known to be absorbed by the epoxy, leading to a significant reduction in the SIL's transparency [40].

The dispensed UV-curable polymer can be tuned, using one of two methods. The first and most simple is to exploit the polymer's relatively strong attraction to the substrate to create a larger than required SIL with the correct sized base. The SIL can then be tuned by withdrawing epoxy from the center of the dispensed droplet, allowing the volume to reduce whilst the base's dimensions stay relatively constant. Another method of tuning the shape involves applying a bias between the needle and sample, and using the principle of electro-wetting to change the droplets shape [38–40]. Once the desired shape is obtained the SIL can be cured by exposure to UV light, permanently fixing its location, and shape. The sample can then be removed from the glycerol bath and washed with deionized water to remove any remaining glycerol. Further details on the fabrication process of an epoxy SIL, can be found from [39].
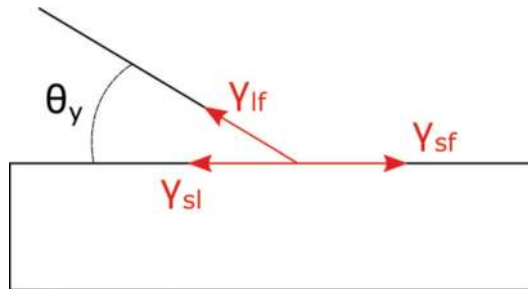

Figure 7. Diagram illustrating Young's equilibrium contact angle (θy), due to the balancing of the solid–liquid (γsl), liquid-filler (γlf) and solid-filler (γsf) surface tensions.

3.2. Enhanced light coupling

Figure 8a shows how a SIL enhances the coupling of light out of a TMD based device. The SIL on the RHS of the blue dashed line refracts the light rays produced by the TMD at the SIL-air boundary closer to the normal leading to more rays entering the lens (shown as a double ended red arrow).

The increase in the coupling of light can be used to increase the light output of a TMD by increasing the solid angle of light that can be observed rather than lost to the environment. **Figure 9a** shows the measured photoluminescence (PL) spectra for a monolayer at 10 μW of excitation power. Comparing the integrated intensity of the flake both before and after the application of a SIL, an increase in PL intensity of 4.0× is observed. This enhancement arises from the SIL refracting light at the SIL-air boundary. A SIL with the dimensions shown in **Figure 8b** should increase the solid angle of light emitted vertically by 1.33×, the SiO_2 layer underneath it will also reflect light back, creating a virtual source which will, in turn be enhanced by the SIL. Calculating these values, we find that the theoretical solid angle of the reflected light would be increased by 3.15×, which when scaled to take account of the percentage of light that would be reflected and added to the vertical emission we get a total enhancement of 2.0 × .

The theoretical enhancement value calculated is only half the power of the experimental results, however, this only considers the coupling of light out of the SIL, and does not consider what happens to the excitation source entering the SIL. A beam of light travelling in
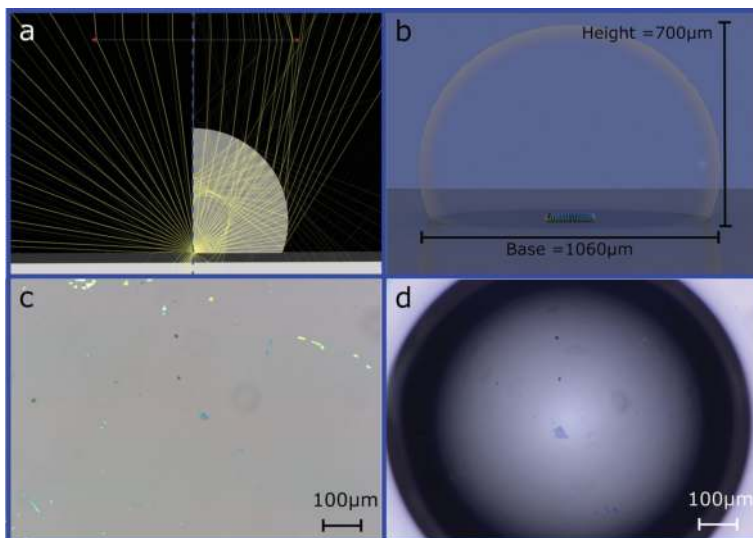

Figure 8. (a) A ray trace simulation demonstrating how the SIL increases the coupling of light, (b): A render of the SIL in c and d from the side with dimensions, (c and d): Microscope images showing an isolated TMD flake both before (c), and after (d) being magnified by a SIL.
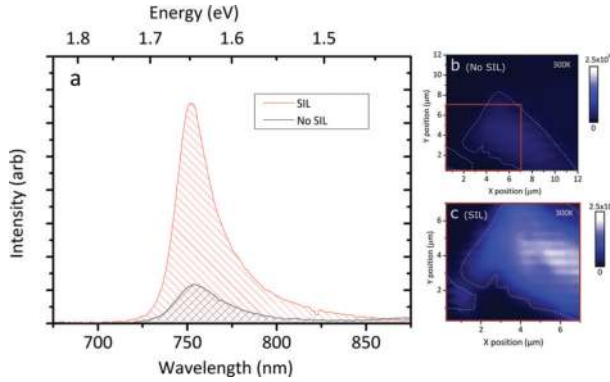
Figure 9. (a) Graph showing the room temperature photoluminescence of a WSe$_2$ monolayer both with and without a SIL, demonstrating the influence of the SIL in improving light collection efficiency. (b and c) Photoluminescence map of the same flake as (a) both without a SIL (b) and with a SIL (c), the intensity scale in these maps are identical, and the orange square in b shows the area in c that has been magnified by the SIL.

air is normally diffraction limited in terms of its size, and can be described by the Rayleigh criterion. When considering a beam being focused through a lens onto a surface we can use the following equation to describe the half-width at half-maximum (FWHM) of the resultant airy pattern:

$$FWHM = \frac{0.52\lambda}{n\,NA_{obj}} \tag{3}$$

where n is refractive index of the medium above the TMDC, NA_{obj} is the numerical aperture of the μPL system and λ is the excitation wavelength [57]. For a 532 nm laser travelling through the air we get a FWHM of 0.42 nm; in contrast a SIL with refractive index of 1.56 (such as the one demonstrated in **Figure 8**) has a FWHM of 2.7 nm. Assuming light is not lost due to scattering/reflection from the SIL then the incident optical power is unchanged, meaning that the power density of the laser spot increases due to the same optical power being focused into a smaller area. This change in power density for the aforementioned SIL translates to a 2.4× increase in light per unit area. Unfortunately, this will not lead to a 2.4× increase in light output of the monolayer WSe$_2$, as the quantum efficiency of WSe$_2$ is typically low [13, 58, 59]. However, the increased excitation will lead to an increase in PL intensity (providing the excitonic ground state does not become saturated), and may explain the difference observed between theory and experimental observations.

Figure 8c and **d** show a 2D flake before and after being magnified through the application of a SIL. This magnification increase arises from the SIL creating an optical lever effect [60] (i.e. moving the focal position laterally across the SIL produces a smaller lateral movement under the SIL). The magnification allows maps to be made with a higher number of measurements per unit area. This can be easily observed from **Figure 9b** and **c** which show PL maps of the emission of a flake without and with a SIL, respectively. Note that both maps have the same number of pixels despite **Figure 9c** showing a map of a smaller area. This increased resolution

is especially important, when pushing the limits of micro-photoluminescence, and can have many optoelectronic applications. In the example of a photodetector, the increased magnification can enable the size of the detector to be reduced, whilst maintaining the same collection area, giving potential reductions in response times and jitter.

The magnification increase from **Figure 8c–d** was found to be 1.8×, indicating that the SIL has a shape between that of a hemisphere (linear dependence with n giving 1.56×) and an ideal super-sphere (quadratic dependence with n giving 2.43×). This result shows that SILs in between the h and s-SIL geometries (shown in **Figure 6**), can give optical properties that are a combination of the two, with the studied SIL showing a greater magnification than an h-SIL without introducing strong chromatic aberrations.

4. Improved device longevity

We have up to this point considered the properties of an epoxy SIL in terms of its optical performance, which although considerable is limited by the epoxy's refractive index. SILs formed from materials like glass can have higher refractive indices, and thus can cause better optical enhancement, and indeed are well suited to coupling light into/out of embedded structures with a flat surface over them. However, due to being solid and having a large hardness, glass SILs are unsuitable for coupling light into/out of sensitive photo-absorbers/emitters like 2D materials, as their presence risks damage to the flake and is likely to leave an air gap that will significantly degrade its optical performance. Epoxy formed SILs do not suffer from this problem as the SIL can be formed over the sensitive structure as a liquid, then hardened into a solid to fully encapsulate the emitter. This hardening process causes no damage to the emitter and fully seals the emitter away from any physical or chemical harm, giving the epoxy SILs a significant advantage over other types of SILs.

Encapsulation can be essential for materials that have finite lifetimes in an ambient environment. The photoluminescence of emitters such as colloidal quantum dots (CQD's) [61, 62] and monolayer TMD's are strongly suppressed when exposed to oxidants and organic contaminants present in the air [63–65]. In the case of TMD's this strong suppression of PL is accompanied by a large change in the flake's structure and morphology especially at grain boundaries [66]. Strategies such as encapsulation with hexagonal boron nitride (h-BN) have been shown to be effective at preventing this oxidization [67] however, this form of encapsulation adds complexity and cost to the potential manufacturing processes. Photopolymers such as UV cured epoxies are commonly used in the mass-manufacture of products [68] and should also seal the TMD from oxygen. To test this hypothesis, a monolayer of WSe_2 was encapsulated within a SIL and its appearance and PL intensity measured over several months in ambient conditions (a time period known to cause a reduction in PL [69]). The results of this experiment are shown in **Figure 10**, the total integrated PL of the peak was found to stay constant within error over 5 months. In addition, the inset microscope images show that there are no visible changes in the monolayers appearance, suggesting that the SIL encapsulation helps to prolong the emissive lifetime of a monolayer in ambient conditions.
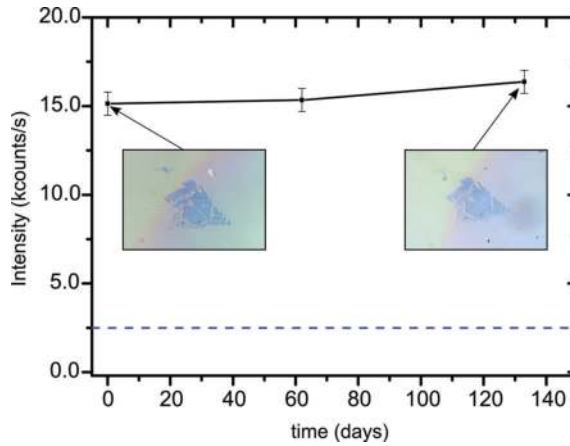
Figure 10. Graph showing the change in photoluminescence intensity with time, for a flake of WSe$_2$ immersed within an epoxy SIL (the dashed blue line shows the peak intensity before application of the SIL).

The enhanced light coupling provided by a SIL combined with the tunability and protective nature of the liquid epoxy that forms makes it an efficient, cheap and scalable solution for the capping of 2D TMD based optoelectronics. Their obvious use is to improve the emission of light emitting devices such as TMD based LED's [8]. Their high magnification and ability to focus light into a structure as well as out of a structure make them valuable for photodetector applications. PhC cavities as we have previously explored are ideal for coupling light into a 2D material based detector; however, they require high NA objective lenses to focus incoming light to a tight enough spot that they can be effectively coupled into the crystal by the output coupler. Mounting a SIL on-top of the PhC, and centered on the coupler can allow much simpler optics to be used as the SIL is providing some of the required magnification.

5. Conclusions and outlook

2D materials have shown great promise for replacing conventional bulk semiconductors in optoelectronic applications such as photodetectors and light emitters [8, 70]. Unfortunately, their low absorption due to their inherent atomic thickness presents limitations in adapting the material for photodetection applications. Here we have reviewed a rod-type PhC cavity structure which increases the light absorption of a 2D material flake coupled spatially to a cavity mode. Coupling the flake to a cavity with a Q-factor of 300 has been shown to be able to increase the material absorption to almost unity which has the potential to eliminate the absorption limitation of 2D material based photodetectors.

Directing collimated light to such a small structure for photodetection applications requires complicated optics such as expensive, high-NA objective lenses. SILs formed using UV-cured epoxy have been shown to magnify a 2D material based structure, this can enable

simpler coupling optics to be utilized. The higher refractive index of the SIL can also help reduce the diffraction limit of a focused spot, helping to couple more light into one area. Hence for optimum efficiency, our proposed scheme for a 2D material based photodetector involves the transfer of a flake on top of a rod-type PhC cavity, and spatial coupling of the monolayer and the cavity mode maximum via the flake's declining into the cavity structure. A UV-curable epoxy SIL is then dispensed on top of the cavity. Dispensing the SIL above the cavity provides three advantages. The first is to help collimate light into a tighter focal spot and magnify the 2D flake to simplify coupling optics. The second is providing an encapsulation of the 2D material to isolate it from the external environment, thereby increasing its longevity and improving its optical performance. The third advantage of dispensing a UV-cured epoxy SIL over the PhC cavity is enhancing the Q-factor of the cavity by reflecting vertically leaking light back into the cavity due to the refractive index contrast between the air and epoxy.

Recent work by Bie et al. [30] has shown that TMDs can be used to form a waveguide-integrated light source and photodetector based on a p-n junction. This novel scheme enables the photoresponsivity of the detector to be tuned and the scheme reversed for realizing a 2D material coupled to hole-PhC LED. The advantage of this scheme is that one device can perform two roles. Using this concept with rod-type PhC coupled to SILs can provide an increase in material's absorption for a photodetection mode as well as greatly increasing the light output of the LED mode. Opening new doors to niche applications and technologies.

Acknowledgements

Author details

Yasir J. Noori*, Christopher S. Woodhead and Robert J. Young

*Address all correspondence to: yasir.noori@gmail.com

Department of Physics, Lancaster University, Lancaster, UK

References

[1]   Ferrari AC, Bonaccorso F, Fal'ko V, et al. Science and technology roadmap for graphene, related two-dimensional crystals, and hybrid systems. Nanoscale. 2015;**7**(11):4598-4810. DOI: 10.1039/c4nr01600a

[2]   Quesnel E, Roux F, Emieux F, et al. Graphene-based technologies for energy applications, challenges and perspectives. 2D Materials. 2015;**2**(3):030204. DOI: 10.1088/2053-1583/2/3/030204

[3]   Furchi MM, Pospischil A, Libisch F, et al. Photovoltaic effect in an electrically tunable van der Waals heterojunction. Nano Letters. 2014;**14**(8):4785-4791. DOI: 10.1021/nl501962c

[4]   Radisavljevic B, Radenovic A, Brivio J, et al. Single-layer MoS2 transistors. Nature Nanotechnology. 2011;**6**(3):147-150. DOI: 10.1038/nnano.2010.279

[5]   Lee J, Mak KF, Shan J. Electrical control of the valley hall effect in bilayer MoS2 transistors. Nature Nanotechnology. 2016;**11**(5):421-425. DOI: 10.1038/nnano.2015.337

[6]   Wachter S, Polyushkin DK, Bethge O, et al. A microprocessor based on a two-dimensional semiconductor. 2017;**8**:14948. DOI: 10.1038/ncomms14948

[7]   Fiori G, Bonaccorso F, Iannaccone G, et al. Electronics based on two-dimensional materials. Nature Nanotechnology. 2014;**9**:768. DOI: 10.1038/nnano.2014.207

[8]   Withers F, Del Pozo-Zamudio O, Mishchenko A, et al. Light-emitting diodes by band-structure engineering in van der Waals heterostructures. Nature Materials. 2015;**14**(3):301-306. DOI: 10.1038/nmat4205

[9]   Lopez-Sanchez O, Lembke D, Kayci M, et al. Ultrasensitive photodetectors based on monolayer MoS2. Nature Nanotechnology. 2013;**8**:497. DOI: 10.1038/nnano.2013.100

[10]   Sarkar D, Liu W, Xie X, et al. MoS2 field-effect transistor for next-generation label-free biosensors. ACS Nano. 2014;**8**(4):3992-4003. DOI: 10.1021/nn5009148

[11]   Yameng C, Alexander JR, Abdullah A, et al. Optical identification using imperfections in 2D materials. 2017;**4**(4):045021. DOI: 10.1088/2053-1583/aa8b4d

[12]   Alharbi A, Armstrong D, Alharbi S, et al. Physically unclonable cryptographic primitives by chemical vapor deposition of layered MoS2. ACS Nano. 2017. DOI: 10.1021/acsnano.7b07568

[13]   Amani M, Lien D-H, Kiriya D, et al. Near-unity photoluminescence quantum yield in MoS2. Science. 2015;**350**(6264):1064. DOI: 10.1126/science.aad2114

[14]   Schnitzer I, Yablonovitch E, Caneau C, et al. Ultrahigh spontaneous emission quantum efficiency, 99.7% internally and 72% externally, from AlGaAs/GaAs/AlGaAs double heterostructures. Applied Physics Letters. 1993;**62**(2):131-133. DOI: 10.1063/1.109348

[15] Gauck H, Gfroerer TH, Renn MJ, et al. External radiative quantum efficiency of 96% from a GaAs/GaInP heterostructure. Applied Physics A. 1997;**64**(2):143-147. DOI: 10.1007/s003390050455

[16] Tonndorf P, Schmidt R, Böttger P, et al. Photoluminescence emission and Raman response of monolayer MoS2, MoSe2, and WSe2. Optics Express. 2013;**21**(4):4908-4916. DOI: 10.1364/OE.21.004908

[17] Kang K, Xie S, Huang L, et al. High-mobility three-atom-thick semiconducting films with wafer-scale homogeneity. Nature. 2015;**520**:656. DOI: 10.1038/nature14417

[18] Ansari N, Moradi M. Optical absorption in air/monolayer MoS2/S (SSiO2 or Si) trilayer stacks at oblique incidence. Superlattices and Microstructures. 2017;**104**(Supplement C):104-111. DOI: 10.1016/j.spmi.2017.02.010

[19] Kim H, Lien D-H, Amani M, et al. Highly stable near-unity photoluminescence yield in monolayer MoS2 by fluoropolymer encapsulation and superacid treatment. ACS Nano. 2017;**11**(5):5179-5185. DOI: 10.1021/acsnano.7b02521

[20] Alharbi A, Zahl P, Shahrjerdi D. Material and device properties of superacid-treated monolayer molybdenum disulfide. Applied Physics Letters. 2017;**110**(3):033503. DOI: 10.1063/1.4974046

[21] Zeng S, Hu S, Xia J, et al. Graphene–MoS2 hybrid nanostructures enhanced surface plasmon resonance biosensors. Sensors and Actuators B: Chemical. 2015;**207**:801-810. DOI: 10.1016/j.snb.2014.10.124

[22] Wang Z, Dong Z, Gu Y, et al. Giant photoluminescence enhancement in tungsten-diselenide-gold plasmonic hybrid structures. Nature Communications. 2016;**7**. DOI: 10.1038/ncomms11283

[23] Sobhani A, Lauchner A, Najmaei S, et al. Enhancing the photocurrent and photoluminescence of single crystal monolayer MoS2 with resonant plasmonic nanoshells. Applied Physics Letters. 2014;**104**(3):031112. DOI: 10.1063/1.4862745

[24] Lee KCJ, Chen Y-H, Lin H-Y, et al. Plasmonic gold nanorods coverage influence on enhancement of the photoluminescence of two-dimensional MoS2 monolayer. Scientific Reports. 2015;**5**:16374. DOI: 10.1038/srep16374

[25] Kim J, Son H, Cho DJ, et al. Electrical control of optical plasmon resonance with graphene. Nano Letters. 2012;**12**(11):5598-5602. DOI: 10.1021/nl302656d

[26] Johnson AD, Cheng F, Tsai Y, et al. Giant enhancement of defect-bound exciton luminescence and suppression of band-edge luminescence in monolayer WSe2–Ag plasmonic hybrid structures. Nano Letters. 2017;**17**(7):4317-4322. DOI: 10.1021/acs.nanolett.7b01364

[27] Akselrod GM, Weidman MC, Li Y, et al. Efficient nanosecond photoluminescence from infrared PbS quantum dots coupled to plasmonic nanoantennas. ACS Photonics. 2016;**3**(10):1741-1746. DOI: 10.1021/acsphotonics.6b00357

[28] Duan H, Fernández-Domínguez AI, Bosman M, et al. Nanoplasmonics: Classical down to the nanometer scale. Nano Letters. 2012;**12**(3):1683-1689. DOI: 10.1021/nl3001309

[29] Emani NK, Chung T-F, Ni X, et al. Electrically tunable damping of plasmonic resonances with graphene. Nano Letters. 2012;**12**(10):5202-5206. DOI: 10.1021/nl302322t

[30] Bie Y-Q, Grosso G, Heuck M, et al. A MoTe2-based light-emitting diode and photodetector for silicon photonic integrated circuits. Nature Nanotechnology. 2017. DOI: 10.1038/nnano.2017.209

[31] Noori YJ, Cao Y, Roberts J, et al. Photonic crystals for enhanced light extraction from 2D materials. ACS Photonics. 2016;**3**(12):2515-2520. DOI: 10.1021/acsphotonics.6b00779

[32] Furchi M, Urich A, Pospischil A, et al. Microcavity-integrated graphene photodetector. Nano Letters. 2012;**12**(6):2773-2777. DOI: 10.1021/nl204512x

[33] Majumdar A, Kim J, Vuckovic J, et al. Electrical control of silicon photonic crystal cavity by graphene. Nano Letters. 2013;**13**(2):515-518. DOI: 10.1021/nl3039212

[34] Mansfield SM, Kino GS. Solid immersion microscope. Applied Physics Letters. 1990;**57**(24):2615-2616. DOI: 10.1063/1.103828

[35] Yoshita M, Sasaki T, Baba M, et al. Application of solid immersion lens to high-spatial resolution photoluminescence imaging of GaAs quantum wells at low temperatures. Applied Physics Letters. 1998;**73**(5):635-637. DOI: 10.1063/1.121931

[36] Vamivakas AN, Younger RD, Goldberg BB, et al. A case study for optics: The solid immersion microscope. American Journal of Physics. 2008;**76**(8):758-768. DOI: 10.1119/1.2908186

[37] Zwiller V, Björk G. Improved light extraction from emitters in high refractive index materials using solid immersion lenses. Journal of Applied Physics. 2002;**92**(2):660-665. DOI: 10.1063/1.1487913

[38] Jin X, Guerrero D, Klukas R, et al. Microlenses with tuned focal characteristics for optical wireless imaging. Applied Physics Letters. 2014;**105**(3):031102. DOI: 10.1063/1.4890967

[39] Woodhead CS, Roberts J, Noori YJ, et al. Increasing the light extraction and longevity of TMDC monolayers using liquid formed micro-lenses. 2D Materials. 2017;**4**(1):015032. DOI: 10.1088/2053-1583/4/1/015032

[40] Born B, Landry EL, Holzman JF. Electrodispensing of microspheroids for lateral refractive and reflective photonic elements. IEEE Photonics Journal. 2010;**2**(6):873-883. DOI: 10.1109/JPHOT.2010.2076800

[41] Yablonovitch E. Inhibited spontaneous emission in solid-state physics and electronics. Physical Review Letters. 1987;**58**(20):2059-2062. DOI: 10.1103/PhysRevLett.58.2059

[42] Astratov VN, Bogomolov VN, Kaplyanskii AA, et al. Optical spectroscopy of opal matrices with CdS embedded in its pores: Quantum confinement and photonic band gap effects. Il Nuovo Cimento D. 1995;**17**(11):1349-1354. DOI: 10.1007/BF02457208

[43] Krauss TF, Rue RMDL, Brand S. Two-dimensional photonic-bandgap structures operating at near-infrared wavelengths. Nature. 1996;**383**:699. DOI: 10.1038/383699a0

[44] Busch K, von Freymann G, Linden S, et al. Periodic nanostructures for photonics. Physics Reports. 2007;**444**(3):101-202. DOI: 10.1016/j.physrep.2007.02.011

[45] Hennessy K, Badolato A, Winger M, et al. Quantum nature of a strongly coupled single quantum dot-cavity system. Nature. 2007;**445**:896. DOI: 10.1038/nature05586

[46] Wu S, Buckley S, Schaibley JR, et al. Monolayer semiconductor nanocavity lasers with ultralow thresholds. Nature. 2015;**520**:69. DOI: 10.1038/nature14290

[47] Liu T, Qiu H, Yin T, et al. Enhanced light-matter interaction in atomically thin MoS2 coupled with 1D photonic crystal nanocavity. Optics Express. 2017;**25**(13):14691-14696. DOI: 10.1364/OE.25.014691

[48] Sanfeng W, Sonia B, Aaron MJ, et al. Control of two-dimensional excitonic light emission via photonic crystal. 2D Materials. 2014;**1**(1):011001

[49] Gan X, Gao Y, Mak KF, et al. Controlling the spontaneous emission rate of monolayer MoS2 in a photonic crystal nanocavity. Applied Physics Letters. 2013;**103**(18):181119. DOI: 10.1063/1.4826679

[50] Ye Y, Wong ZJ, Lu X, et al. Monolayer excitonic laser. Nature Photonics. 2015;**9**(11):733-737. DOI: 10.1038/nphoton.2015.197

[51] Villeneuve PR, Fan S, Joannopoulos JD. Microcavities in photonic crystals: Mode symmetry, tunability, and coupling efficiency. Physical Review B. 1996;**54**(11):7837-7842. DOI: 10.1103/PhysRevB.54.7837

[52] Paton KR, Coleman JN. Relating the optical absorption coefficient of nanosheet dispersions to the intrinsic monolayer absorption. Carbon. 2016;**107**(Supplement C):733-738. DOI: 10.1016/j.carbon.2016.06.043

[53] Kay ND, Robinson BJ, Fal'ko VI, et al. Electromechanical sensing of substrate charge hidden under atomic 2D crystals. Nano Letters. 2014;**14**(6):3400-3404. DOI: 10.1021/nl500922h

[54] Johnson SG, Fan S, Villeneuve PR, et al. Guided modes in photonic crystal slabs. Physical Review B. 1999;**60**(8):5751-5758. DOI: 10.1103/PhysRevB.60.5751

[55] Qian W, Ghislain LP, Elings VB. Imaging with solid immersion lenses, spatial resolution, and applications. Proceedings of the IEEE. 2000;**88**(9):1491-1498. DOI: 10.1109/5.883320

[56] Frieder M, Jean-Christophe B. Electrowetting: From basics to applications. Journal of Physics. Condensed Matter. 2005;**17**(28):R705. DOI: 10.1088/0953-8984/17/28/R01

[57] Moehl S, Zhao H, Don BD, et al. Solid immersion lens-enhanced nano-photoluminescence: Principle and applications. Journal of Applied Physics. 2003;**93**(10):6265-6272. DOI: 10.1063/1.1567035

[58] Mak KF, Shan J. Photonics and optoelectronics of 2D semiconductor transition metal dichalcogenides. Nature Photonics. 2016;**10**(4):216-226. DOI: 10.1038/nphoton.2015.282

[59] Mak KF, Lee C, Hone J, et al. Atomically thin MoS$_2$: A new direct-gap semiconductor. Physical Review Letters. 2010;**105**(13):136805

[60] Serrels KA, Ramsay E, Dalgarno PA, et al. Solid immersion lens applications for nanophotonic devices. Journal of Nanophotonics. 2008;**2**(1):021854-021829. DOI: 10.1117/1.3068652

[61] Shirasaki Y, Supran GJ, Bawendi MG, et al. Emergence of colloidal quantum-dot light-emitting technologies. Nature Photonics. 2013;**7**(1):13-23. DOI: 10.1038/nphoton.2012.328

[62] Igor LM, Uyeda HT, Ellen RG, et al. Quantum dot bioconjugates for imaging, labelling and sensing. Nature Materials. 2005;**4**(6):435. DOI: 10.1038/nmat1390

[63] Sang-Yul P, Hyo-Sun K, Jeseung Y, et al. Long-term stability of CdSe/CdZnS quantum dot encapsulated in a multi-lamellar microcapsule. Nanotechnology. 2015;**26**(27):275602. DOI: 10.1088/0957-4484/26/27/275602

[64] Roberto CL, Rafik A, Santosh KC, et al. Intrinsic air stability mechanisms of two-dimensional transition metal dichalcogenide surfaces: Basal versus edge oxidation. 2D Materials. 2017;**4**(2):025050. DOI: 10.1088/2053-1583/aa636c

[65] Gao J, Li B, Tan J, et al. Aging of transition metal dichalcogenide monolayers. ACS Nano. 2016;**10**(2):2628-2635. DOI: 10.1021/acsnano.5b07677

[66] Rong Y, He K, Pacios M, et al. Controlled preferential oxidation of grain boundaries in monolayer tungsten disulfide for direct optical imaging. ACS Nano. 2015;**9**(4):3695-3703. DOI: 10.1021/acsnano.5b00852

[67] Ahn S, Kim G, Nayak PK, et al. Prevention of transition metal dichalcogenide photo-degradation by encapsulation with h-BN layers. ACS Nano. 2016;**10**(9):8973-8979. DOI: 10.1021/acsnano.6b05042

[68] Crivello JV, Reichmanis E. Photopolymer materials and processes for advanced tech-nologies. Chemistry of Materials. 2014;**26**(1):533-548. DOI: 10.1021/cm402262g

[69] He Z, Wang X, Xu W, et al. Revealing defect-state photoluminescence in monolayer WS2 by cryogenic laser processing. ACS Nano. 2016;**10**(6):5847-5855. DOI: 10.1021/acsnano.6b00714

[70] Koppens FHL, Mueller T, Avouris P, et al. Photodetectors based on graphene, other two-dimensional materials and hybrid systems. Nature Nanotechnology. 2014;**9**:780. DOI: 10.1038/nnano.2014.215